

# Photon-echo studies of collective absorption and dynamic localization of excitation in conjugated polymers and oligomers

Xiujuan Yang,\* Tienieke E. Dykstra,\* and Gregory D. Scholes†

Lash-Miller Chemical Laboratories, 80 St. George Street, University of Toronto, Toronto, Ontario, M5S 3H6 Canada

(Received 20 May 2004; revised manuscript received 28 September 2004; published 7 January 2005)

Investigations of the origins of line broadening and excited state dynamics for the conjugated polymer poly[2-methoxy,5-(2-ethyl-hexoxy)-1,4-phenylenevinylene] (MEH-PPV) and a model pentamer, *p*-bis{[*o,m*-di(2-ethylhexy)oxy-*p*-methylstyryl]styryl}benzene are reported. The time-integrated three-pulse stimulated echo peak shift (3PEPS) experiment is employed to elucidate dephasing, spectral inhomogeneity arising from conformational disorder, and dynamical processes, otherwise obscured by ensemble averaging. We progressively discuss three dynamical models to describe the experimental data. The multiphonon model describes coupling of the electronic transitions to high frequency vibrational modes, and is able to fit the absorption spectra well, highlighting the importance of a distribution of conjugation length. However, it fails to model the 3PEPS data. A two-level system approach is found to reproduce the absorption line shapes as well as 3PEPS data, however, it cannot simultaneously describe the fluorescence data since the homogeneous linewidth is grossly overestimated. In light of these analyses, we propose the three-stage relaxation model, that (1) describes absorption into delocalized states that arise from electronically coupled conformational subunits; (2) explains the fast decay of the 3PEPS data as a rapid dynamic localization of excitation; and (3) provides a homogeneous line broadening that is consistent for both the absorption and fluorescence processes. Simultaneous modeling of the 3PEPS, absorption, and fluorescence data, establishes a consistent picture to understand the line broadening, dephasing mechanisms, and excited state dynamics for conjugated polymers and oligomers.

DOI: 10.1103/PhysRevB.71.045203

PACS number(s): 78.47.+p, 78.66.Qn, 78.40.-q, 71.35.-y

## I. INTRODUCTION

Poly (*p*-phenylene vinylene) (PPV), its derivatives, such as poly [2-methoxy, 5-(2'-ethyl-hexoxy)-1,4-phenylene vinylene] (MEH-PPV), and its oligomers represent new types of materials compared to small organic molecules.<sup>1-5</sup> Although employed in efficient electroluminescent devices, their photophysical properties are not completely understood. Characteristics of these conjugated polymers and oligomers are high luminescence quantum yields, large apparent Stokes' shifts, broad absorption bands, and nonmirror image absorption and fluorescence spectra. A model that satisfactorily explains all these phenomena has not been elucidated.

Theoretical studies have suggested the importance of torsional motions and changes in molecular structure that underlie dynamical processes induced upon photoexcitation.<sup>6</sup> Understanding of the elementary excitations and dynamics in conjugated polymers appears to be a central subject enabling design, optimization, and tuning at the molecular level of devices based on conjugated polymers. For example, controlling conformational disorder or length of polymer chain can profoundly affect the luminescence yield and charge transport efficiency and therefore the overall efficiency of OLED devices.<sup>7-15</sup> In the present work we report a microscopic model that qualitatively and quantitatively describes the origins of conjugated polymer photophysics. We elucidate this model by comparing the origins of line broadening in the conjugated polymer MEH-PPV with the model pentamer, *p*-bis{[*o,m*-di(2-ethylhexy)oxy-*p*-methylstyryl]styryl}benzene (Fig. 1). We show that the basic characteristics of conjugated polymers are derived from

those of conformational subunits. However, these conformational subunits may couple to contribute collective electronic states to the absorption spectrum. Subsequent to absorption, these collective states are rapidly localized by conformational relaxation. This provides an important new viewpoint on the role, significance and nature of conformational subunits.

Although conjugated polymers share some similarities with inorganic semiconductors, they differ in that the properties of conjugated polymers are apparently characterized by an interplay of  $\pi$ -system conjugation lengths and conformational disorder owing to the relatively low energy barrier for disruptive small angle rotations around  $\sigma$ -bonds along the

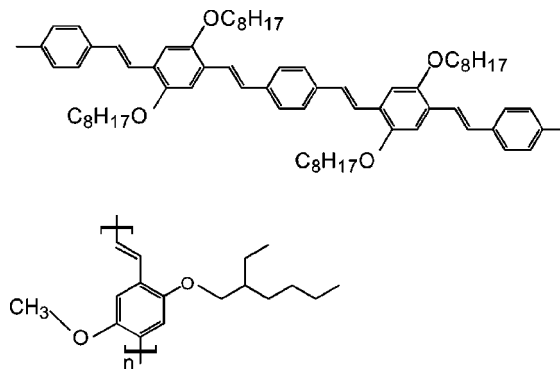


FIG. 1. Molecular structures of the pentamer, *p*-bis{[*o,m*-di(2-ethylhexy)oxy-*p*-methylstyryl]styryl}benzene and the conjugated polymer poly[2-methoxy,5-(2'-ethyl-hexoxy)-1,4-phenylene vinylene] (MEH-PPV).

backbone of conjugated chains.<sup>16–25</sup> The distribution function of different conjugation lengths takes a Gaussian form with the center estimated to be five subunits, constituting an ensemble of polyene-type electronic oscillators.<sup>26–29</sup> Such information is contained in the linear absorption spectrum together with the homogeneous absorption line shape contribution manifested by the coupling between electronic transitions and nuclear motions, causing fluctuations and relaxations of electronic transition energies.<sup>1,30</sup> The time scales and amplitude of these fluctuations together dictate dephasing processes and characterize the dynamical width of fluctuations of the electronic energy gap (absorption line shape).<sup>31</sup> A detailed understanding of the absorption line shape for small organic molecules in the condensed phase has been ascertained.<sup>32–39</sup> Previous work has shown that the origin of line shape in conjugated polymers differs fundamentally from such model two level systems.<sup>1,26–29</sup> For example, it is possible that interplay between conformational subunits predicted by the Coulomb interaction affects the optical properties and electronic structure of conjugated polymers.

Many investigations have addressed the linear and nonlinear optical properties of conjugated polymers.<sup>2,40–45</sup> Time-resolved absorption, fluorescence, and transient grating have been applied to study excited state dynamics. Time-resolved absorption and transmission spectroscopy has provided some information on the initial relaxation processes occurring after photoexcitation,<sup>46–48</sup> such as the strong coupling between electronic and vibrational states in excited state dynamics. Femtosecond fluorescence experiments revealed an ultrafast relaxation of optical excitations within an inhomogeneously broadened density of states. However, unemitted relaxation is possibly not detected. In order to establish connections between conformational disorder, optical line shape and photophysics, an experimental approach that is sensitive to a suitable correlation function, rather than population dynamics, is required.

The three-pulse stimulated echo peak shift (3PEPS) measurement is widely used to obtain time scales of solvation and protein dynamics owing to its great dynamic range—from femtoseconds to nanoseconds.<sup>32–39,49–52</sup> The peak shift reflects the rephasing and echo formation capability of the medium. Thus 3PEPS is capable of providing much valuable information, such as all the time scales of dephasing processes that are coupled to an electronic transition, by providing a line shape function and separating homogeneous and inhomogeneous broadening.<sup>31–35,53,54</sup> Here, we apply 3PEPS to investigate signatures of dephasing characteristic of MEH-PPV and the model pentamer. Using this spectroscopy we have been able to elucidate the details of line shape broadening as a correlation function. The work we report here has revealed that motions involving structural reorganization within individual conformational subunits dominate the homogeneous line shape.

We have developed a three-stage relaxation model in order to explain the origins of inhomogeneous line broadening and to simultaneously model the 3PEPS, absorption and fluorescence line shapes.

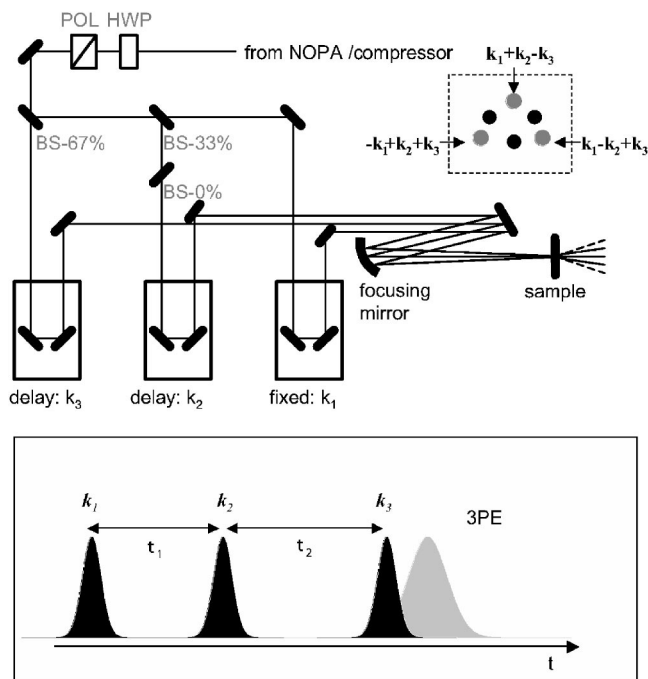


FIG. 2. Experiment setup and pulse sequence for the 3PEPS experiment. See the text for details.

## II. EXPERIMENT

A tunable nonlinear optical parametric amplifier (NOPA) was pumped by 200  $\mu\text{J}$  of the output of a Ti:sapphire regeneratively amplified laser system that generates  $\sim 140$  fs pulses at 775 nm and 1 kHz. The tunable visible output of the NOPA was used for excitation.<sup>55</sup> The excitation wavelength was centered at 485 nm (2.56 eV) for the pentamer and 538 nm (2.31 eV) for MEH-PPV samples. The intensities of the excitation beams were controlled by using a half-wave plate/polarizer combination. Dispersion was precompensated using a pair of quartz prisms. The resulting ultrafast pulse duration was measured by autocorrelation at the sample position according to the intensity FWHM of the sum frequency generation in a 50  $\mu\text{m}$  BBO crystal (assuming a Gaussian pulse shape). The pulse durations were estimated to be 20–40 fs depending on excitation wavelength. Time-bandwidth products were 0.44 and 0.59, respectively. The laser spectrum was measured using a CVI SM-240 CCD spectrometer.

3PEPS measurements were performed using three beams of equal intensity ( $\sim 5$  nJ/beam at the sample), Fig. 2. The three *S*-polarized beams were aligned after the delay stages to form an equilateral triangle beam geometry (1 cm sides) and were focused into the sample using a silver-coated spherical mirror ( $f=25$  cm). The symmetric sweep delay control was used for the 3PEPS measurement. Two beams were independently delayed to scan pulse delays from negative  $\tau$ , pulse sequence 2-1-3, to positive  $\tau$ , pulse sequence 1-2-3, such that the population time  $T$  is fixed between pulses 1 and 3 at  $\tau < 0$  and then between 2 and 3 at  $\tau > 0$ .

The three-pulse echo signals in the  $-k_1+k_2+k_3$  and  $k_1-k_2+k_3$  phase matching directions were spatially isolated us-

ing irises and measured simultaneously. The peak shift  $\tau^*$  for each population time  $T$  corresponds to the coherence time  $\tau$  when the time-integrated photon echo signals peak. The temporal overlap between the three pulses was set initially by autocorrelating each of the three pulse pairs. Accurate  $T=0$ , and  $\tau=0$  stage positions were set according to overlap of the pulses in the sample by measuring all three three-pulse echo signals and using the symmetry of the echo signals along the  $\tau$  time axis. The time delay between pulse 1 and 2 was set using  $-k_1+k_2+k_3$  and  $k_1-k_2+k_3$  signals. The delay between pulse 2 and 3 was set using  $k_1-k_2+k_3$  and  $k_1+k_2-k_3$  signals.

The first pulse, with wave vector  $k_1$ , creates an electronic coherence between ground and excited states. The second pulse,  $k_2$ , creates a population which is allowed to undergo dynamic processes for a time  $T$ . The last pulse  $k_3$ , converts the population into a coherence which generates an echo in the  $k_s=-k_1+k_2+k_3$  phase matching direction. Simultaneously, we measure the signal with wave vector  $k'_s=+k_1-k_2+k_3$  (with pulse sequence 2-1-3). Peak positions of the measured echo signal were obtained by fitting each of the two data traces with a Gaussian function. The echo signals are symmetric along the  $\tau$  axis at room temperature, so the peak shift  $\tau^*$  for each  $\tau$ -scan at a fixed  $T$  was accurately determined by taking half the separation between the peaks of the Gaussian fits for the two signal directions. The peak shift is expressed by  $\tau^*=(|\tau_1^*|+|\tau_2^*|)/2$ .

Chlorobenzene (spectroscopic grade) was obtained from Aldrich Chemical Company. MEH-PPV was purchased from Aldrich. The model pentamer was provided by Professor Lewis Rothberg, University of Rochester. Solutions of MEH-PPV and pentamer in chlorobenzene were filtered to remove insoluble impurities. The absorbance was adjusted to be 0.2 in a 100  $\mu\text{m}$  cell. The solutions were circulated through a 100  $\mu\text{m}$  flow cell using a gear pump. All measurements reported here were conducted at 294 K.

### III. RESULTS

Absorption and photoluminescence spectra of dilute MEH-PPV and pentamer solutions (chlorobenzene solvent) at room temperature are shown in Fig. 3. Both the pentamer and MEH-PPV have broad, unstructured absorption bands and narrower, structured fluorescence spectra. The maximum of the absorption band of the pentamer solution is located at  $\sim 435$  nm (2.85 eV) while the apparent Stokes' shift between the absorption and fluorescence band peaks is  $\sim 2600$   $\text{cm}^{-1}$  (322 meV). MEH-PPV has a broader, redshifted absorption band compared to the pentamer. The absorption maximum is at  $\sim 500$  nm (2.48 eV) in chlorobenzene, the apparent Stokes' shift is  $\sim 2330$   $\text{cm}^{-1}$  (289 meV). The similarity of the spectra for the two samples suggests that the primary origins of the line broadening in the absorption spectra do not differ greatly. This is somewhat surprising given that static inhomogeneity reflecting conformational disorder is anticipated to contribute significantly to the MEH-PPV absorption spectrum. This conformational disorder is further discussed in Sec. V.

Figure 4 shows the time integrated 3PE signal at various population times for the pentamer and MEH-PPV in chlo-

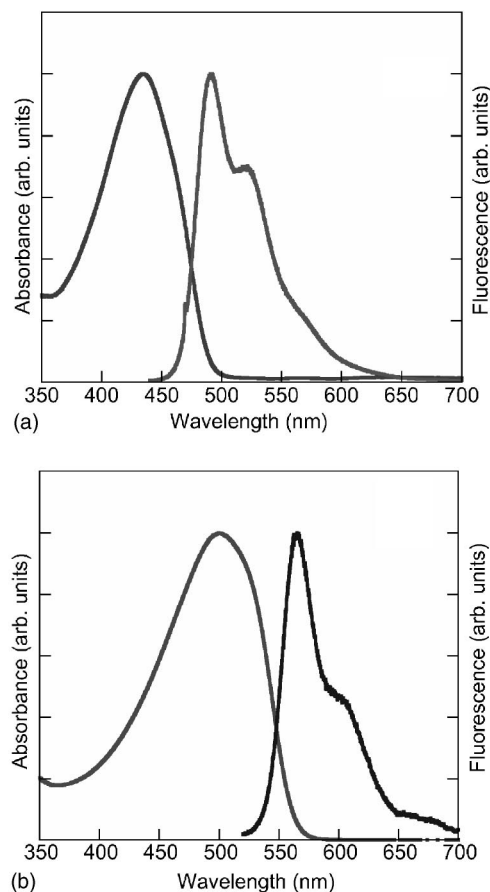


FIG. 3. Absorption and photoluminescence spectra of pentamer (a) and MEH-PPV (b) in chlorobenzene solution. Slit widths were 1.5 nm. Excitation wavelengths were 450 nm and 520 nm, respectively.

robenezene solutions. The 3PE data in upper panels for the pentamer are obtained using laser pulses with center wavelength at 485 nm, and pulse duration of 45 fs FWHM. For MEH-PPV the excitation center wavelength is 538 nm, with a laser pulse duration of 25 fs FWHM. The 3PE signals are pulse-width limited, and the actual peak shift is affected by pulse duration.<sup>35</sup> The effect of pulse duration on peak position is accounted for in the simulation of the signals.

The 3PEPS experiment gives us the information that is contained in the 3PE signals in a compact form. 3PEPS reveals information about the time scales of dephasing and is sensitive to a correlation function. In order to understand the rather complicated data, we must perform computer simulations. However, it is possible to interpret the 3PEPS data qualitatively. Disorder in the system is manifested in the 3PEPS data as an asymptotic peak shift; the larger the offset, the larger the disorder. Although influenced by pulse-width and solvent effects, a higher initial peak shift is associated with weaker coupling, as shown in Fig. 5.

The relationship between asymptotic peak shift and  $T$ , the population time, can be understood using the following equation for the asymptotic peak shift:<sup>31</sup>

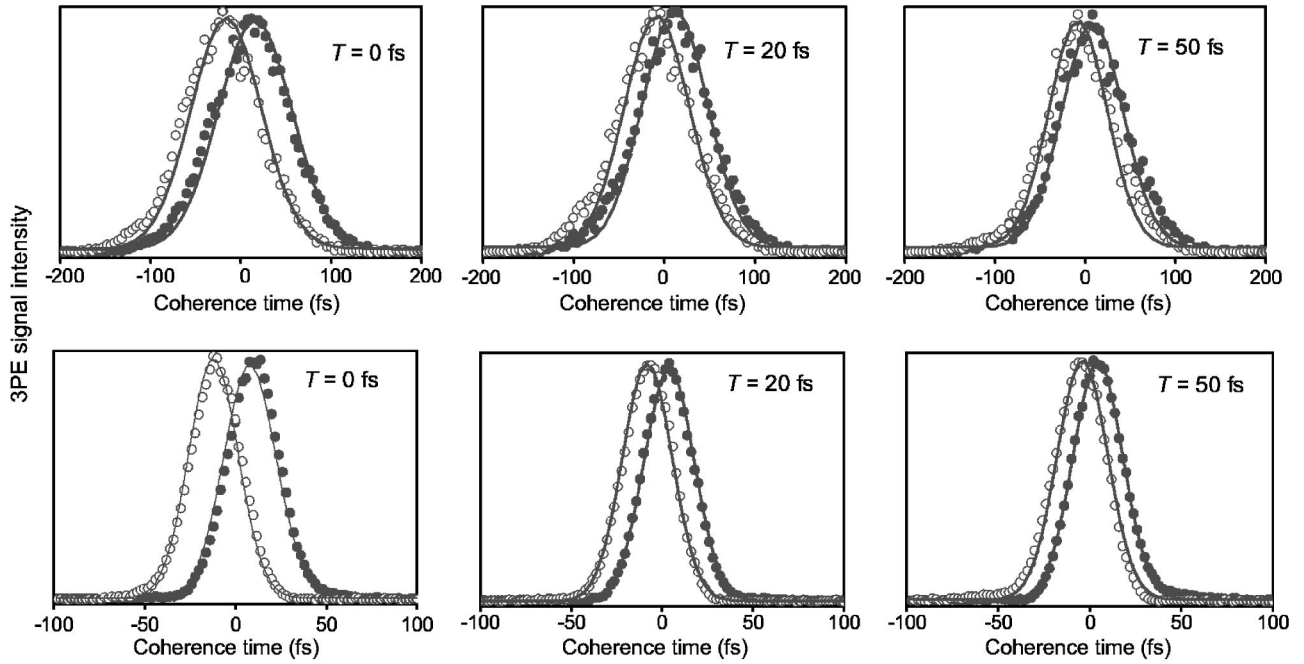


FIG. 4. 3PE signal versus coherence time for population times  $T=0, 20,$  and  $50$  fs, for both the pentamer (upper panels) and MEH-PPV (lower panels) in chlorobenzene. Open circles are the data for the phase matching direction  $k_1-k_2+k_3$  and the filled circles are for the phase matching direction  $-k_1+k_2+k_3$ . The solid lines represent the Gaussian fit of the echo data points. As the population time is increased, the peak shift decreases.

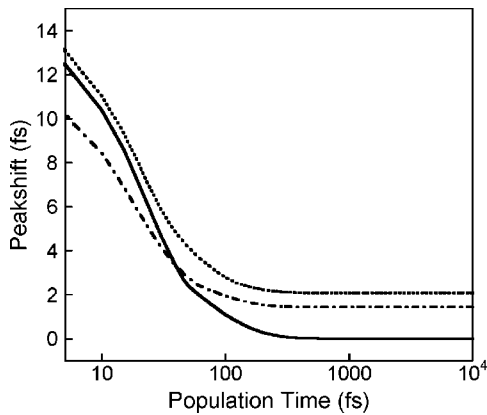


FIG. 5. Example of 3PEPS data. The peak shift provides a measure of the inhomogeneity of the frequency distribution. Strong coupling to the bath increases the homogeneous broadening, correspondingly reducing the peak shift. These data were simulated using the full response function. The solid lines are 3PEPS data simulated using an exponential  $M(t)$  with  $\tau_e=100$  fs and  $\lambda_e=900$   $\text{cm}^{-1}$ . This represents Kubo relaxation. To demonstrate the effect of disorder in the system, a static Gaussian contribution is added to that  $M(t)$ , with  $\sigma=1000$   $\text{cm}^{-1}$ . Those simulated 3PEPS data are shown by the dotted line. Note that now a long-time, asymptotic peak shift is evident. The effect of increased coupling to the bath is demonstrated by simulating the 3PEPS data with this  $M(t)$ , but now with  $\lambda_e=1100$   $\text{cm}^{-1}$ . There is a decrease in the initial peak shift and the asymptotic offset (dashed-dotted line).

$$\tau^*(T \rightarrow \infty) = \frac{\sigma_{in}^2 \sqrt{\Gamma + \sigma_{in}^2 + \lambda^2}}{\sqrt{\pi} [\Gamma(\Gamma + 2\sigma_{in}^2 + \lambda^2) + \sigma_{in}^2 \lambda^2]}, \quad (1)$$

where  $\Gamma=2\lambda/(\hbar\beta)$  and  $\beta=1/kT$ .  $\lambda$  is the total reorganization energy divided by  $\hbar$ .  $\sigma_{in}$  is the static inhomogeneity of the system. When  $\sigma_{in} \neq 0$  a nonzero peak shift is observed. It can also be shown that the peak shift decays as  $M(t)$ , the correlation function for fluctuations of the electronic energy gap, in the absence of static inhomogeneity.<sup>31</sup> The form of  $M(t)$  will be discussed in greater detail in the following sections.

3PEPS data  $\tau^*$  versus population time,  $T$  for the pentamer and MEH-PPV in chlorobenzene solution are plotted in Fig. 6(a) and 6(b), respectively. The primary amplitude of the peak shift data for both pentamer and MEH-PPV rapidly decays within  $T=500$  fs, attaining a persistent offset at a population time of 5 ps. It is clear that MEH-PPV has a higher asymptotic offset than that of pentamer. This result is reproducible under different sample, pulse-width, and experimental setup conditions. The nonzero persistent peak shift is attributed to the degree of structural defects along the conjugated backbone. Looking at the  $T < 500$  fs population time region, it is evident that the pentamer 3PEPS data decays more slowly compared to MEH-PPV. The clear and slowly diminishing oscillations in the pentamer 3PEPS data are due to the coherently excited intramolecular vibrations that are weakly damped by the bath. The oscillations for MEH-PPV are washed out by many averaged excited vibrational modes since the frequency of these vibrations depends on the size of the conformational subunits.<sup>56,57</sup>

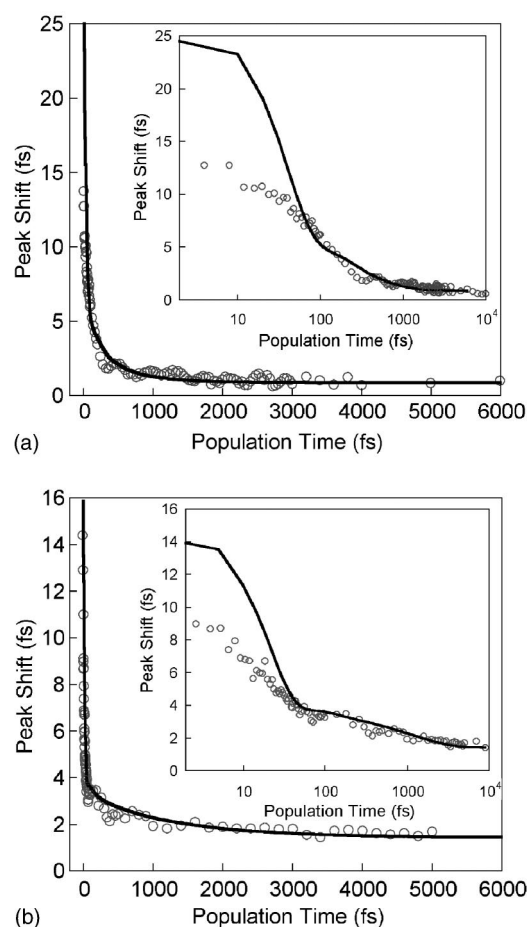


FIG. 6. 3PEPS data,  $\tau^*$  vs population time for the pentamer (a) and MEH-PPV (b) in chlorobenzene. Solid lines are simulated data using the three-stage relaxation model [Eq. (21)]. The insets show the same data on a log- $x$  scale.

#### IV. THE STOKES' SHIFT

There has been much investigation into the nonmirror image relationship between absorption and fluorescence and the large difference between the absorption and emission maxima observed in conjugated polymers. In the following section, we will introduce three major contributors to the apparent Stokes' shift, some of which also affect the mirror image/line shape, and which can be examined using different spectroscopic techniques. They are the true molecular Stokes' shift arising from electron-phonon coupling, an ultrafast localization component, and spectral diffusion through energy transfer.

##### A. Molecular Stokes' shift and spectral diffusion

The coupling of electronic transitions to a bath of fluctuating nuclei in any chromophore effects line broadening and the Stokes' shift. Often we consider the characteristic time scales of bath fluctuations to label line broadening as homogeneous or inhomogeneous. Homogeneous line broadening results from a fluctuating frequency distribution; inhomoge-

neous broadening denotes an effectively static frequency distribution. It is also illustrative to consider the spectral density, to gain insight into the connection between reorganization energy and the Stokes' shift via fluctuation dissipation. This spectral density is essentially the distribution of time scales (frequencies) weighted by coupling constants.<sup>54</sup>

The energy gap for an electronic transition of a chromophore is influenced by the fluctuations in the environment and the chromophore itself. Assuming that the fluctuations are similar for all chromophores in the system, the time-dependent Stokes' shift

$$S(t) = \frac{\langle \delta V_{SB}(t) \delta V_{SB}(0) \rangle}{\langle \delta V_{SB}^2 \rangle} \quad (2)$$

with  $\delta V_{SB}$  as the system-bath fluctuation, can be expressed in terms of the spectral density as follows:<sup>34</sup>

$$S(t) = \hbar/\lambda \int_0^\infty d\omega \rho(\omega) \cos \omega t, \quad (3)$$

where  $\omega$  is the frequency of the fluctuations,  $\rho(\omega)$  is the spectral density.  $\lambda$  is a renormalization constant which is identical to the reorganization energy

$$\lambda = \hbar \int_0^\infty d\omega \omega \rho(\omega). \quad (4)$$

The line shape function can be expressed in the frequency domain as<sup>31,58</sup>

$$g(t) = -i\lambda t/\hbar + \int_0^\infty d\omega \rho(\omega) \coth[\hbar\omega\beta/2] (1 - \cos \omega t) + i \int_0^\infty d\omega \rho(\omega) \sin \omega t, \quad (5)$$

where  $\beta = 1/kt$ .

These expressions yield the Stokes' shift and line shapes in the absence of energy transfer and generally pertain to isolated chromophores. Clearly, there is a fundamental relationship between homogeneous line broadening and the Stokes' shift ( $2\lambda$ ). On the other hand, inhomogeneous line broadening does not contribute to fluctuations of each chromophore transition frequency and therefore does not affect the Stokes' shift. In order to obtain molecular Stokes' shifts in more complex systems such as conjugated polymers, special spectroscopic techniques must be used. For example, by selectively exciting only the red-most chromophores, site selective fluorescence techniques reveal the molecular Stokes' shift, unaffected by spectral diffusion associated with energy transfer.<sup>59-61</sup>

##### B. Coupled chromophores and dynamic localization

The ideas of localization and delocalization of electronic states<sup>62,63</sup> are known to be important in the study of photosynthetic systems, and we will demonstrate in this paper that they also play a role in the photophysics of conjugated polymers. The absorption of excitation onto the B850 band of the

2light harvesting complex LH2 of purple bacteria and the subsequent localization onto a single dimer pair is an illustrative example.<sup>64</sup> In this well studied system, there have been numerous experiments and discussions as to the extent of delocalization observed. The answer seems to be that different experiments interrogate different time scales and thus show different degrees of localization of excitation. It has been calculated that there are strong electronic couplings between the 18 chromophores in the B850 band and thus absorption excites excitonic states. Circular dichroism experiments (CD) provide an incisive probe of the instant of excitation, and thus absorption of a photon into delocalized states of the B850 ring, for example. In fact, in order to account for observed CD spectra, delocalization over at least half the ring system is required.<sup>65,66</sup> On the other hand, the extent of delocalization is found to be much less when calculating the super-radiance from fluorescence experiments in the same systems.<sup>67</sup> Fluorescence measurements are sensitive to times cales on the order of the fluorescence lifetimes, suggesting a localization of excitation *before* emission. It is predicted, therefore, that emission would occur from localized states while absorption is into delocalized exciton states.<sup>68</sup>

The 3PEPS experiment has a sufficiently large dynamic range to be sensitive to all of these time scales.<sup>32–39,49–52,69</sup> We are, therefore, able to monitor the dynamics of localization as well as other, slower processes, such as resonance energy transfer.<sup>70,71</sup>

### C. Resonance energy transfer

There are two distinct regimes of energy transfer important to the study of conjugated polymers. The first is the rapid localization, already discussed, whose associated spectral diffusion gives rise to part of the apparent Stokes' shift. The second, slower process is likely to operate via a generalized-Förster mechanism where energy is transferred from a localized excitation on the donor to a delocalized "aggregate chromophore" state.<sup>72–75</sup> Owing to the separation of time scales, energy transfer (from donor chromophore to delocalized chromophore aggregate) occurs well after the initial localization of excitation. However, this is still shorter than the fluorescence lifetime. Multiple localization-energy transfer to delocalized acceptor-localization processes may occur before fluorescence is observed from excitation localized on the lowest energy chromophores in the system.<sup>59–61</sup>

## V. SIMULATION OF THE DATA

We have simulated the data using three models. The multiphonon model gives a physical picture of conjugated poly-

mers and conformational subunits. It is able to fit the absorption line shape. However, this model, in its present form, is unable to fit the 3PEPS, reinforcing the issue of the insensitivity of linear absorption to the origins of line broadening. To simulate the 3PEPS and absorption simultaneously, we have used a two-level electronic system approach derived from studies of solvation. However, this approach does not satisfactorily fit the fluorescence line shape. To incorporate spectral diffusion through the inhomogeneously broadened density of states, we move to the three-stage relaxation model. Within this model, we are able to simulate the 3PEPS signal as well as the absorption and fluorescence line shapes.

### A. Multiphonon model

Previous work suggests that the distribution of conjugation lengths of phenylene-based molecular systems is determined by conformational disorder in the system and that the distribution function is Gaussian.<sup>26</sup> In this section, we present and discuss the simulations of the absorption spectrum of MEH-PPV by a theoretical approach<sup>26</sup> that is derived from molecular radiationless transition theory.<sup>76,77</sup> The simulation of absorption is based on the properties of each conjugation segment which, when superimposed, form the MEH-PPV absorption profile.<sup>78</sup> In the Frenkel exciton theory, a conjugated system with  $N$  units can have energies

$$E_l = E_0 + 2\beta \left( \frac{\pi l}{N+1} \right), \quad (6)$$

where  $l=1, 2, \dots, N$ ,  $E_0$  is the energy of excited state of each unit and  $\beta$  is the interaction strength between nearest-neighbor conjugation units. The corresponding transition dipole moment is

$$|\vec{\mu}_N^l| = \frac{2|\vec{\mu}|^2}{N+1} \left[ \cot \left( \frac{\pi l}{2N+2} \right) \right]^2, \quad (7)$$

where the monomer dipole moment  $|\vec{\mu}|^2=1$ . The absorption coefficient  $\alpha_{eg}(\omega)$  for the electronic transition  $g \rightarrow e$  of each conjugation segment is given by

$$\alpha_{eg}(\omega) = \frac{2\pi\omega}{3ac\hbar} |\mu_{eg}|^2 \int_{-\infty}^{\infty} dt \left[ \frac{it}{\hbar} (E_e - E_g - \hbar\omega) - \frac{1}{2}d^2t^2 \right] \times \exp \left[ - \prod_j G_j(t) \right], \quad (8)$$

where  $\mu_{eg}$  denotes the electronic transition moment.  $a$  is the factor which describes the medium effect,  $c$  is the speed of light,  $d$  is the width of inhomogeneity of electronic states, and here  $\prod_j G_j(t)$  corresponds to the line shape function, which is defined via

$$G_j(t) = \frac{2\beta_j\beta_j' \sinh(\hbar\omega_j/2kT)}{\sinh \lambda_j \sinh \mu_j''} \frac{\exp[-\beta_j^2\beta_j'^2\Delta_j^2/[\beta_j'^2 \coth(\lambda_j/2) + \beta_j^2 \coth(\mu_j''/2)]]}{\sqrt{[\beta_j'^2 \coth(\mu_j''/2) + \beta_j^2 \coth(\lambda_j/2)][\beta_j'^2 \tanh(\mu_j''/2) + \beta_j^2 \tanh(\lambda_j/2)]}}. \quad (9)$$

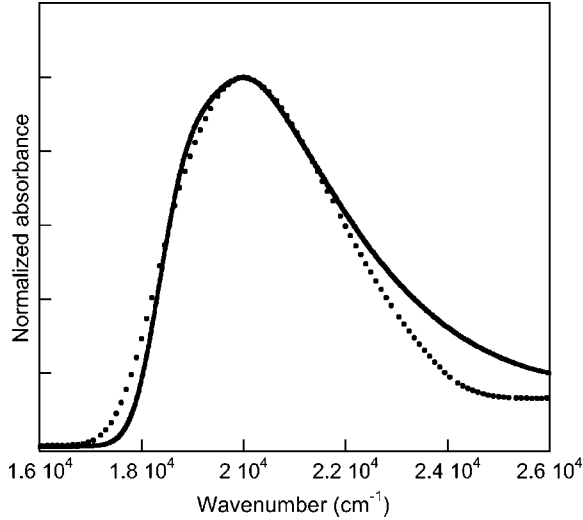


FIG. 7. Simulation of MEH-PPV absorption line shape by the multiphonon model [Eq. (11)] (dotted line). Solid line is experimental data.

In Eq. (9),  $\beta_j = (\omega_j/\hbar)^{1/2}$ ,  $\lambda_j = i\tau\omega_j + \hbar\omega_j/2kT$ ,  $\mu_j'' = -i\tau\omega_j''$ , where  $\omega_j$  and  $\omega_j''$  are the oscillator frequencies of the  $j$ th mode in the electronic states  $g$  and  $e$ , respectively,  $\Delta_j$  denotes the normal coordinate displacement which is chosen so that the conjugation length ( $N$ ) dependent Huang-Rhys factor  $S_j = \omega_j\Delta_j^2/2\hbar = a_j + b_j/(N+1)$  with  $a_j$  and  $b_j$  being adjustable, as described by Chang *et al.*<sup>26</sup> We take the Gaussian function  $D[N]$  deduced from the disorder to describe the distribution of conjugation segments of MEH-PPV backbone with center  $N_0$  and width  $B_{av}$  as fitting parameters. In our calculation, the best fit for absorption spectrum of MEH-PPV gives us  $N_0 = 5$  and  $B_{av} = 6.3$ ,

$$D[N] = B_{av}^{-1/2} \exp[-(N - N_0)^2/B_{av}]. \quad (10)$$

Thus, the molecular absorption coefficient for MEH-PPV is given by

$$\alpha(\omega) = \sum_N D[N] \alpha_{e_N g_N}(\omega) \quad (11)$$

The calculated absorption spectrum of MEH-PPV is shown in Fig. 7 with contributions from conjugation segments consisting of one to nine subunits compared with experimental data. As in Ref. 26, the blue tail of the absorption spectrum is fitted by choosing 1400 (1550), 700 (700), and 200 (200)  $\text{cm}^{-1}$  for the three vibrational modes of the ground (excited) state of each conjugation segment. The slight discrepancy between the experimental data and the simulation is probably due to underestimating the contribution from the short conjugation length segments. The width of inhomogeneity  $d$  is taken as 900  $\text{cm}^{-1}$  for all segments.

The multiphonon model can fit the absorption line shape well. However, the calculation of  $G_j(t)$  includes only high frequency modes, since we do not have detailed information on the distribution of low frequency torsional modes. This means that the homogeneous broadening, influenced by low frequency modes in the spectral density, is not taken into

account in this model. Thus the line shape function  $\Pi_j G_j(t)$  of Eq. (9) cannot fit our 3PEPS data to obtain the line broadening response function, which is indispensable to differentiate between homogeneous and inhomogeneous broadening. Moreover, there seem to be subtleties missing from the multiphonon model, in its present form, that are necessary to understand the pentamer data. The following two-level electronic system approach allows this differentiation by describing these low frequencies in the bath spectral density according to a Brownian oscillator model.

### B. Two-level electronic system approach

Assuming that the coupling between the electronic transition of each conjugation segment is coupled to a bath of nuclei which are undergoing Brownian motion, we use a two-level electronic system to model the chromophore-bath system. The theoretical treatment of third-order nonlinear optical signals has been described elsewhere in detail.<sup>58,79</sup> The electronic energy gap between ground and excited states for an individual conjugation segment  $i$  can be separated into its averagetransition frequency  $\langle\omega\rangle$ , a dynamical fluctuating term  $\delta\omega_i(t)$  and a static offset  $\epsilon_i$ .

$$\omega_i(t) = \langle\omega\rangle + \delta\omega_i(t) + \epsilon_i. \quad (12)$$

The time-integrated 3PE signal  $S(T, \tau)$  measured in the laboratory is expressed in terms of response functions  $R(t, T, \tau)$  which generate third order polarizations,<sup>58</sup> with  $\tau$  being the time delay between the first two pulses (the coherence period),  $T$  the time delay between the last two pulses (the population period), and  $t$  the time evolution of nonlinear polarization after the third pulse,

$$S(T, \tau) = \int_0^\infty dt |R(t, T, \tau)|^2. \quad (13)$$

For a 3PEPS experiment, the peak shift  $\tau^*(T)$  at a particular time  $T$  is defined as the coherence time at which the integrated echo signal is a maximum. The behavior of  $\tau^*(T)$  is closely related to the transition frequency correlation function  $M(t)$ .<sup>31,35</sup>

The nonlinear response function can be expanded in terms of line shape function  $g(t)$  as described by Mukamel and co-workers.<sup>79–82</sup>  $g(t)$  is in turn related to the correlation function  $M(t)$ , which accounts, in this approach, for bath fluctuations in the condensed phase. The line shape function  $g(t)$  is defined via

$$g(t) = -i\lambda \int_0^t dt_1 M(t_1) + \langle\delta\omega^2\rangle \int_0^t dt_1 \int_0^{t_1} dt_2 M(t_2). \quad (14)$$

From this function, we obtain absorption and fluorescence line shape functions,

$$\sigma_A(\omega) = \int_{-\infty}^\infty dt \exp[-i(\omega - \omega_{eg})t] \exp[-g(t)], \quad (15)$$

$$\sigma_F(\omega) = \int_{-\infty}^{\infty} dt \exp[-i(\omega - \omega_{eg} + 2\lambda)t] \exp[-g^*(t)]. \quad (16)$$

In order to obtain information concerning the amplitude and time scales of the fluctuations of the bath, as well as the inhomogeneity of the system, we have modeled our data using the unnormalized correlation function  $M(t)$  as a sum of components as follows:

$$M(t) = \sum \lambda_e \exp(-t/\tau_e) + \lambda_{\text{vib}} \exp(-t/\tau_{\text{vib}}) \cos(\omega_{\text{vib}}t + \phi) + \sigma_i^2, \quad (17)$$

where  $\lambda_e$  are the reorganization energies associated with exponential contributions that model Brownian fluctuations with time scales (correlation times)  $\tau_e$ .  $\lambda_{\text{vib}}$  is vibrational reorganization energy of the vibrational mode with the damping time  $\tau_{\text{vib}}$ .  $\lambda$  is related to the amplitude of the fluctuations at temperature  $T$  by

$$\lambda = \frac{\langle \delta\omega^2 \rangle}{2kT}. \quad (18)$$

The coupling of low-frequency vibrational modes to the electronic transition is taken into account to fit the data according to exponential terms in Eq. (17). It has been determined in previous Raman spectra analysis that the low frequency mode has a large Huang-Rhys factor  $S$ , and hence the sum of  $S\omega_{\text{vib}}$  controls the huge apparent Stokes' shift of phenylenevinylene oligomers.<sup>83</sup> Leng *et al.* ascribe the low frequency modes to torsional modes of PPV polymer and its derivatives.<sup>41</sup>

In general, the inertial motion in solvation is caused by the small angle free rotation of a few solvent molecules, and has been shown to be well approximated by a Gaussian component of  $M(t)$ .<sup>34,84,85</sup> We cannot include a Gaussian contribution to  $M(t)$  and retrieve an acceptable simulation of the experimental 3PEPS data. The absence of this component in the simulations of the polymer and pentamer is an indication that dephasing in both these materials is not governed by solvation, but has a different origin.

Static inhomogeneity owing to the distribution of conjugation lengths and isomers derived from conformational disorder is assumed to follow a Gaussian distribution, and is included in the correlation function according to a standard deviation  $\sigma_i$ . This is an important contributor to broadening of the absorption line shape, and as we will show in the following section, helps to explain the nonmirror image relationship between absorption and emission.

3PEPS data for the pentamer in chlorobenzene were found to be fit best by  $M(t)$  with two exponential components  $\lambda_{ej} \exp(-t/\tau_{ej})$ , with  $\lambda_{e1}=170 \text{ cm}^{-1}$  and  $\tau_{e1}=25 \text{ fs}$ ;  $\lambda_{e2}=1130 \text{ cm}^{-1}$  and  $\tau_{e2}=690 \text{ fs}$ . The sum of the coupling strength was fixed to be  $1300 \text{ cm}^{-1}$  according to the experimentally determined apparent Stokes' shift for the pentamer in chlorobenzene ( $2600 \text{ cm}^{-1}$ ). The coherently excited intramolecular vibrations were simulated as damped cosines  $\lambda_{\text{vib}} \exp(-t/\tau_{\text{vib}}) \cos(\omega_{\text{vib}}t + \phi)$ , with  $\lambda_{\text{vib}}=40 \text{ cm}^{-1}$  and  $\tau_{\text{vib}}=4 \text{ ps}$ ,  $\omega_{\text{vib}}=80 \text{ cm}^{-1}$ , and  $\phi=1.8 \text{ rad}$ . The static inhomoge-

neity required to reproduce the data was found to be  $\sigma_i=1200 \text{ cm}^{-1}$ . The appearance of slowly damped oscillations indicates weak coupling between electronic transition and solvent bath.

3PEPS data for MEH-PPV in chlorobenzene were modeled using the response function  $M(t)$ , which is best represented by three exponentials  $\lambda_{ej} \exp(-t/\tau_{ej})$ . We obtained  $\lambda_{e1}=250 \text{ cm}^{-1}$  and  $\tau_{e1}=5 \text{ fs}$ ;  $\lambda_{e2}=610 \text{ cm}^{-1}$  and  $\tau_{e2}=70 \text{ fs}$ ;  $\lambda_{e3}=300 \text{ cm}^{-1}$  and  $\tau_{e3}=1 \text{ ps}$ . The total coupling strengths were also constrained to be  $1160 \text{ cm}^{-1}$  in order to equal one-half of the Stokes' shift estimated from the difference in the peak maxima of the absorption and emission spectra ( $1160 \text{ cm}^{-1}$ ). The small offset shown in the data required a static inhomogeneity,  $\sigma_i=1000 \text{ cm}^{-1}$ . The vibrational contribution with a frequency  $80 \text{ cm}^{-1}$  for the pentamer is assigned to torsional motion. Analogous vibrations are damped out in the polymer data owing to the superposition of vibrational modes from the distribution of conjugation lengths.

Discrepancies between calculated and experimental spectra and the form of energy gap transition correlation function prompted us to scrutinize contributions to the 3PE signal. According to the 3PEPS data and simulations for either pentamer or MEH-PPV, we conclude that any inertial solvation effect is insignificant. The huge coupling strengths and very rapid time constants for all exponential components also exclude diffusive solvation effects typical of dilute chromophore solutions. These observations clearly differentiate the spectroscopy of conjugated polymers from that of dye molecules in solution. An important observation was that using this two-level system model we were unable to fit the fluorescence line shape, which we should have been able to do, given the  $M(t)$  obtained from the 3PEPS experiment.

It is well accepted that the torsional barrier around single bonds in conjugated chains is very low (on the order of  $kT$ ), and the conformational rotation of a conjugation segment is strongly coupled to the electronic transition. For example, Tretiak *et al.* calculated energy profiles of ground and excited states of PPV conjugated polymers, and modeled the excited state of PPV by a planar structure relative to a torsionally disordered ground state conformation.<sup>6</sup> Thus the large apparent Stokes' shift can be interpreted in terms of the conformational change upon excitation, and hence the origin of fluctuation and relaxation of transition energies contained in  $M(t)$  is mostly connected to these conformational changes. On the other hand, the static offsets may represent an extremely long lifetime component that is also related to different conformational changes, such as *cis-trans* transitions along polymer backbone.

The time scales of correlation between conjugation segments that cause dephasing, as well as the coupling between torsional motions and electronic transitions enter the 3PEPS signal. Therefore the dephasing processes of conjugated PPV oligomers and polymers need to be further interpreted by a detailed model for third-order response of a many-body disordered system. In the following section we describe how we can implement this in a phenomenological model.

### C. Three-stage relaxation model

It is apparent from the above analysis that the line shape of MEH-PPV is poorly described as a simple two-level elec-

tronic system coupled to nuclear motions of a solvent bath. Thus, even individual conformational subunits, or the model pentamer, are very much unlike typical chromophores in the condensed phase. We describe here a refined physical model that explains all our observations. This model accounts for (1) absorption into delocalized electronic states; (2) implicit incorporation of the coupling of torsional motions to electronic transitions, and therefore dynamic localization of excitation; (3) coupling to torsional motions and bath fluctuations that provide homogeneous line broadening; (4) inhomogeneous line broadening owing to a distribution of conformational subunits. A particularly significant result is that different manifestations of (1) and (2) in absorption, 3PEPS and other transient spectroscopies,<sup>86</sup> has, up to this point, obfuscated analysis of excited state dynamics.

An understanding of conjugated polymers begins with a clear description of the sources of inhomogeneous line broadening. The physical picture of the polymer is a chain of “wormlike” conjugated segments separated by breaks in conjugation (caused by a large dihedral angle).<sup>21,27</sup> As a result, there is a distribution of conjugation lengths, and for MEH-PPV the average value for conjugation length is approximately five repeat units.<sup>26–29</sup> The distribution of conjugation lengths is influenced by the degree of conformational disorder in the system.<sup>87</sup>

Our experiments suggest that there is another type of disorder manifest in the absorption spectrum. This disorder, represented by standard deviation  $\sigma_1$ , reflects a set of delocalized states formed by Coulombic interactions between proximate conformational subunits. For polyindenofluorene, for example, intrachain electronic couplings are estimated to be in the range 1 to 900  $\text{cm}^{-1}$ ; depending on the length of the conformational subunits.<sup>74</sup> Smaller conformational subunits couple more strongly than larger conformational subunits. Interchain couplings are larger. Thus it is not unreasonable to consider several coupled conformational subunits to constitute a primary absorbing unit.

However, we expect these delocalized states to be very short lived owing to the large reorganization energies characteristic of individual conformational subunits.<sup>6,88</sup> Thus 3PEPS decays according to localization of the excitation, driven by geometrical relaxation of a conformational subunit. Fluorescence emission derives from the relaxed, equilibrated geometry. Thus we introduce the notion that conjugated polymers contain dynamic chromophore/fluorophore units as a consequence of the strong dependence of electronic structure on nuclear coordinates.

Within the framework of a three-stage relaxation model, the inhomogeneity seen in an absorption spectrum is derived from two sources:  $\sigma_1$ , an inhomogeneously broadened density of exciton states and  $\sigma_2$ , the conformational disorder. They are related to the total inhomogeneity,  $\Sigma$ , by:<sup>64</sup>

$$\Sigma^2 = \sigma_1^2 + \sigma_2^2. \quad (19)$$

Figure 8 shows schematically the density of states and the conformational disorder and labels each of the stages of relaxation: absorption, localization, and fluorescence.

The absorption line shape is governed by the correlation function,

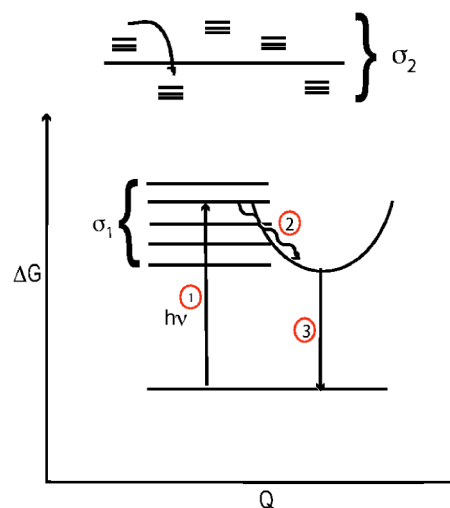


FIG. 8. Origins of inhomogeneity in the three-stage relaxation model. The absorption (1) occurs into a manifold of delocalized states.  $\sigma_1$  is the standard deviation of this inhomogeneously broadened density of exciton states.  $\Sigma$  is the total inhomogeneous line broadening in the absorption spectrum. Subsequent to photoexcitation, there is spectral diffusion (2) through this density of states associated with a rapid localization of excitation.  $\sigma_2$  is the remaining standard deviation of the inhomogeneous broadening, directly related to the conformational disorder. Fluorescence (3) is from a smaller ensemble of localized states as a result of resonance energy transfer.

$$M(t) = \sum \lambda_e \exp(-t/\tau_e) + \lambda_{\text{vib}} \exp(-t/\tau_{\text{vib}}) \cos(\omega_{\text{vib}}t + \phi) + \Sigma^2, \quad (20)$$

where the  $\lambda_e$  are the intramolecular reorganization energies for relaxation with time scales  $\tau_e$ . The vibrational component is the same as in the two-level system. We have ascertained that the homogeneous line broadening is dominated by fluctuations due to the changes in geometry associated with the torsions within conformational subunits. To model that, we have adopted an Ohmic spectral density and exponential  $M(t)$  in keeping with work done by Mukamel and colleagues regarding Kubo's stochastic theory of line shape.<sup>89,90</sup> A key assumption in our analysis is that the homogeneous line shape function—the exponential component in  $M(t)$ —is the same in each measurement. Since absorption pertains to a delocalized excitation and 3PEPS and fluorescence to localizing/localized excitation, this approximation amounts to assuming the local and nonlocal fluctuations are correlated. A considerably more sophisticated model is necessary to account properly for changes in  $g(t)$  during localization of excitation.<sup>91,92</sup>

The massive change in geometry associated with photoexcitation of conjugated polymers and oligomers gives rise to the homogeneous line shape. For PPV oligomers, Tretiak *et al.*<sup>6</sup> modeled the transition to a mainly planar excited state from a ground state with large torsional disorder. This large geometry change, which is also very likely observed upon excitation of MEH-PPV and the model pentamer to the first

singlet excited state, may be viewed as a type of “reaction” along a potential surface.<sup>6,93</sup>

Subsequent to excitation into a delocalized manifold of electronic states, ultrafast relaxation, associated with localization of excitation, is observed in the 3PEPS experiment. The ultrafast relaxation may be interpreted via a random walk within the inhomogeneously broadened density of states.<sup>94</sup> Chromophore fluctuations and dynamics are related to a correlation function, to which the 3PEPS experiment is sensitive, by the fluctuation-dissipation theorem. Owing to the significant difference between ground and excited state equilibrium geometries, an initially photoexcited conformational subunit is far from equilibrium. In response to that, the polymer backbone relaxes through nuclear degrees of freedom into a new equilibrium position. There is a concomitant change in intermolecular configuration.<sup>95</sup> Rather than simply “rolling down” the potential energy surface, the fluctuations and small angle torsions are instrumental in the relaxation process.<sup>96,97</sup> This is manifested as the very fast decay in this stochastic 3PEPS signal. To account for this rapid spectral diffusion we use the phenomenological correlation function given by

$$M(t) = \sum \lambda_e \exp(-t/\tau_e) + \lambda_{\text{vib}} \exp(-t/\tau_{\text{vib}}) \cos(\omega_{\text{vib}}t + \phi) + \sigma_1^2 \exp(-t/\tau_{\text{loc}}) + \sigma_2^2. \quad (21)$$

The homogeneous contribution remains as in the absorption correlation function. The relaxation through the distribution of delocalized states is a dissipative process, thus the additional time-dependent component with amplitude  $\sigma_1^2$ . Hence it is clear that the inhomogeneity  $\sigma_1$  is removed by dynamic localization on a time scale  $\tau_{\text{loc}}$ . The inhomogeneity is associated with conformational disorder is  $\sigma_2$ , which is responsible for the asymptotic offset in the 3PEPS data.

Fluorescence occurs from a small subset of localized states because energy migration through the polymer transfers population to the larger conformational subunits.<sup>59–61,98,99</sup> Thus  $\sigma_2$  narrows to  $\sigma_2'$  prior to emission. The time evolution of  $\sigma_2 \rightarrow \sigma_2'$  is not accounted for explicitly in our simulations because it occurs on longer time scales than we are focussing on. The fluorescence line shape is determined by the correlation function,

$$M(t) = \sum \lambda_e \exp(-t/\tau_e) + \lambda_{\text{vib}} \exp(-t/\tau_{\text{vib}}) \cos(\omega_{\text{vib}}t + \phi) + \sigma_2'^2, \quad (22)$$

where the prime denotes fluorescence from a subset of the entire ensemble. This conformational disorder is much smaller than that required to fit the absorption line shape. In polymers, this may be attributed to resonance energy transfer from the shortest chromophores to the longest (lowest energy) ones.<sup>100</sup> Thus, fluorescence is only observed from this low energy subset of the entire ensemble of chromophores, narrowing the distribution. The picture may be slightly different in the pentamer. Fluorescence is still observed only from a subset of the ensemble, but the origin of this subset can arise from different processes. The poor photostability of the pentamer suggests that photoproducts may be produced. Reaction with oxygen may form ketonic defects, which have been shown to quench fluorescence by migration of energy to the defect.<sup>101,102</sup> Thus, if those pentamers with defects do not fluoresce, the ensemble size of fluorophores is effectively reduced.

Additionally, in order to fit the experimental data, keeping in mind our physical picture of the chromophores, high-frequency modes were added to the simulations of the absorption and fluorescence line shapes. They were incorporated using the following equations for the area-normalized absorption and fluorescence line shapes:<sup>72,103,104</sup>

$$a_i(\epsilon) = \left\langle \sum_i N_a |\mu_i|^2 \sum_k P(k) \text{Re} \int_0^\infty dt \langle k|k(t) \rangle \exp[i(\epsilon - \epsilon_i^k - \lambda)t/\hbar] \exp[-g(t)] \right\rangle \epsilon/n, \quad (23)$$

$$f_i(\epsilon) = \left\langle \sum_i N_f |\mu_i|^2 \sum_k P(k) \text{Re} \int_0^\infty dt \langle k|k(t) \rangle \exp[i(\epsilon - \epsilon_i^k + \lambda)t/\hbar] \exp[-g^*(t)] \right\rangle \epsilon^3, \quad (24)$$

where  $g(t)$  is the line broadening function,  $\lambda$  is the reorganization energy associated with the Stokes' shift,  $\mu$  is the transition moment,  $\epsilon_i^k$  is the transition frequency of the  $i$ th chromophore adjusted for thermal population of the  $k$ th vibrational mode. It is weighted by the Boltzman weighting  $P(k)$ .  $\langle k|k(t) \rangle$  is the time-dependent overlap of the initial vibration  $k$  with its evolution in the excited state and  $N_f$  ( $N_a$ ) is a normalization constant. The angular brackets indicate an ensemble average over  $\Sigma$  or  $\sigma_2'$  for the absorption and fluorescence, respectively. In the absence of high frequency

modes, these equations reduce exactly to Mukamel's line shape functions, Eqs. (15) and (16).

With the three correlation functions in hand, we simultaneously fit the absorption, fluorescence and 3PEPS line shapes. The 3PEPS fits are shown in Fig. 6. The parameters are listed in Table I. The absorption and fluorescence fits are shown in Fig. 9. The different time scales of relaxation shown in  $M(t)$  arise from a variety of intramolecular interactions. The ultrafast component (1) observed in both MEH-PPV and the pentamer may be attributed to the Brownian

TABLE I. Simulation parameters in the three-stage relaxation model for the pentamer (a) and the polymer (b).

(a) Pentamer			(b) MEH-PPV		
$\lambda_e, \text{cm}^{-1}$	$\tau_e, \text{fs}$		$\lambda_e, \text{cm}^{-1}$	$\tau_e, \text{fs}$	
$\lambda_1=250$	400		$\lambda_1=210$	85	
$\lambda_2=150$	690		$\lambda_2=177$	1500	
$\sigma, \text{cm}^{-1}$	$\tau_{\text{loc}}, \text{fs}$	$\Sigma, \text{cm}^{-1}$	$\sigma, \text{cm}^{-1}$	$\tau_{\text{loc}}, \text{fs}$	$\Sigma, \text{cm}^{-1}$
$\sigma_1=350$	60		$\sigma_1=416$	25	
$\sigma_2=455$		574	$\sigma_2=425$		595
$\sigma_2'=175$			$\sigma_2'=10$		

motion of the chromophores themselves, which has a direct effect on the conjugation of the  $\pi$ -electron system. Slower relaxations (2) are due to slower, larger angle torsions and the massive rearrangement between ground and excited state geometries. These resulting linewidths and Stokes' shifts are calculated in the high temperature limit. However, a knowledge of  $M(t)$  permits line shapes to be calculated at any temperature.

Conformational disorder plays a role in the behavior of the polymer, and even the pentamer, via  $\sigma_2$ . That was predicted previously, for oligomers that approach or are greater

than the conjugation length.<sup>27</sup> The three-stage relaxation model has incorporated this effect, along with a distribution of exciton states, to simulate the absorption, fluorescence and 3PEPS data simultaneously.

## VI. DISCUSSION

Compared to single molecules with two level states, the properties of conjugated poly- and oligomers are obviously different owing to diminishing solvation effects. The origin of the absorption line shape lies in the nuclear motion coupled to the electronic degrees of freedom. The collective properties of the chromophores give rise to distinct features which differ from a superposition of contributions from individual conjugation segments.

Though the multiphonon model can fit the absorption line shape of MEH-PPV phenomenologically, the line shape function Eq. (9), in its present form, is not effective when faced with the task of explaining the 3PEPS data because we have used a bath spectral density involving only discrete high frequency vibrational modes. This is not representative of the actual spectral density of the conjugated polymers and oligomers, since their electronic transitions appear to be strongly coupled to a bath of low frequency intramolecular modes—presumably torsions.<sup>60</sup> Nonetheless, this multiphonon model provides a clear connection to the coupling between electronic transitions and intramolecular vibrations, that provides the most satisfactory explanation for the homogeneous line shapes retrieved from analysis of the 3PEPS data using the three-stage relaxation model. Furthermore, if the multiphonon model is modified, as described recently,<sup>86</sup> to include electronic interactions between conformational subunits, then it becomes closely related to our three-stage relaxation model, however, it must first be incorporated into the response function formalism to model the 3PEPS data.

We noticed that the Gaussian distribution function used to model inhomogeneous broadening may under-represent the shortest conformational subunits which contribute to the blue edge of the absorption, causing a deviation from a Gaussian line shape. Some research has shown a distribution function with the shortest repeat units most heavily weighted to be successful in simulation of the absorption spectra in linear polyenes.<sup>22,23</sup> Perhaps this would be a better representation and an improvement over the current model. However, the longer side chains on both MEH-PPV and the pentamer

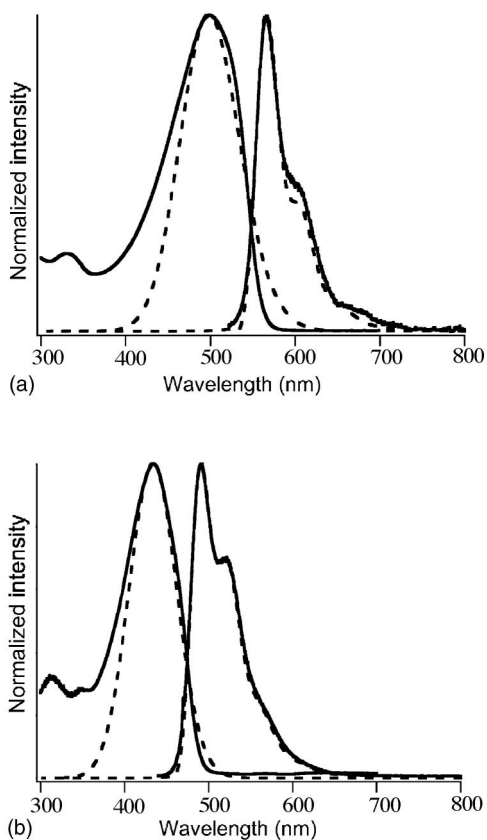


FIG. 9. Simulation of absorption [Eq. (23)] and fluorescence [Eq. (24)] line shapes using the three-stage relaxation model for MEH-PPV (a) and the pentamer (b). Dashed lines are experimental data. Solid lines are simulated data.

would hinder movement more so than in the polyenes, leading to a distribution function somewhat less weighted toward the shortest chromophores.

The two-level system approach works well for other classes of materials, molecular dyes, for example, and was used to simulate the experimental data for MEH-PPV and the pentamer. It provides an approximate description of the low frequency intramolecular modes by assuming them to be continuously distributed and in the high temperature limit. In this model, the distribution of conformational subunits is directly related to the inhomogeneous line broadening of the absorption spectrum and the asymptotic offset of the 3PEPS data. We are able to fit the absorption and 3PEPS line shapes well, however, this model clearly fails when attempting to fit the fluorescence line shape because the homogeneous line broadening is far too large. The two-level system approach does not incorporate relaxation through a broadened density of states. Although, since the time dependence of that localization is exponential, the 3PEPS data can still be simulated by addition of an exponential term to the homogeneous component of the correlation function. However, use of this correlation function is unsatisfactory for simulation of fluorescence data.

The short falls of the two-level system model are remedied by inclusion of a distribution of exciton states in a three-stage relaxation model. Theoretical frameworks have calculated exciton states that derive from the large number of  $\pi$  electrons in conjugated oligomers, although states at the band edge are discrete. Mukamel's collective electronic oscillator approach and the quantum chemical calculations of Beljonne and Brédas are examples.<sup>105–108</sup> We define the manifold of states that leads to the distribution characterized by  $\sigma_1$  as collective states formed by electronic coupling among conformational subunits.<sup>1</sup>

The three-stage relaxation model is a phenomenological model that captures the essential physics of absorption into a delocalized manifold of electronic states, and subsequent evolution to a localized emissive state. It incorporates two types of disorder into the simulations of the absorption, fluorescence and 3PEPS data. In the context of this model, it is apparent that conformational disorder is ultimately responsible for each of these categories of disorder as (i) a distribution of transition frequencies distributed over the polymer; and (ii) a distribution of delocalized exciton states arising from electronic coupling among these subunits. The standard deviation of the distribution of transition frequencies (owing to conformational disorder) is related to the distribution function used in the multiphonon model. Spectral diffusion through an inhomogeneously broadened density of exciton states is included in the simulation of the 3PEPS data to model dynamic localization of excitation. We find this dynamic localization occurs in  $\sim 25$  fs for the polymer. Possible mechanisms by which excitation localizes in conjugated polymers have been discussed recently.<sup>109,110</sup>

The significant geometry change upon photoexcitation (and subsequent relaxation) is intimately related to many of the line shape features of the system. This geometry change itself is very large and has a direct and profound influence on the electronic structure of the polymer by the disruption of  $\pi$  orbitals with nuclear motion. The reorganization energy as-

sociated with this geometry change accounts for nearly all of the observed Stokes' shift. Through the three-stage relaxation model we were able to separate the rapid dynamic localization of excitation from the molecular line shape. We obtain a Stokes' shift corresponding to  $2\lambda \approx 750 \text{ cm}^{-1}$  for MEH-PPV that is comparable to the molecular Stokes' shift reported for poly(phenylphenylenevinylene) of  $500 \text{ cm}^{-1}$ .<sup>61</sup> The reorganization energy,  $\lambda$  is related to the homogeneous line shape by the fluctuation-dissipation theorem.

We view the line broadening in MEH-PPV and the pentamer as arising primarily from coupling to substantial geometry changes, and as such it differs from typical molecules in the condensed phase. Consistent with this picture, the homogeneous line broadening can only be modeled satisfactorily as exponential terms in  $M(t)$ . For example, we were unable to retrieve a Gaussian component associated with inertial solvation. We can consider these nuclear motions to be a bath of overdamped Brownian oscillators. The Stokes' shift, due to relaxation, can only be observed when the oscillators are overdamped. Mukamel shows that in this limit,  $M(t)$  is exponential in nature.<sup>58</sup> Mathies and co-workers have used such an exponential  $M(t)$  in the analysis of the photoisomerization coordinates as a low-frequency vibrational mode with a large Huang-Rhys factor.<sup>93</sup> The transitions of bacteriorhodopsin are strongly coupled to this isomerization coordinate. The example of bacteriorhodopsin is especially relevant given the structural similarity to polyenes.

Mathies and co-workers have shown that the *cis-trans* photoisomerization of bacteriorhodopsin is extremely fast.<sup>93</sup> This is also true of stilbene, the *cis-trans* photoisomerization of which is nearly barrierless along the reaction coordinate.<sup>111,112</sup> In more complex systems, such as conjugated polymers and oligomers in solution, there are many chemically unique double bonds around which photoisomerization may occur. This results in an ensemble of isomers, increasing the inhomogeneity of the system. Vibrational dephasing is expected to occur on a slower time scale and involves coupling of the isomerization coordinate to a wave packet.<sup>111</sup>

It is worthwhile to note that the time-averaged distribution of conjugation lengths remains constant while a "snapshot" of one conformation will differ from the previous, since the system is dynamic. The fluctuations of nuclear coordinates in the chromophores can give rise to inhomogeneous broadening.<sup>113</sup> This is different from the *static* inhomogeneity observed in other systems such as molecular dyes and inorganic semiconductors. The inhomogeneity that provides the asymptotic peak shift observed for both the pentamer and MEH-PPV, may also be caused by a subpopulation of *cis*-isomer photoproducts. Photoisomerization is known to occur in many conjugated systems. Isomerization at any of the carbon sites along the backbone would add to conformational disorder which is manifested as the long-time peak shift offset. The slow interchange between conformations may be another contributor to the residual peak shift observed on the time scale of the experiment. In addition, chains of different conformations have been observed in single molecule studies of MEH-PPV.<sup>114</sup> The presence of *cis*-isomers would support the model that polymers adopt a defect cylinder conforma-

tion in solution.<sup>115</sup> Hairpin turns necessary to form the defect cylinder conformation are easily formed when *cis*-defects are present and are perhaps less accessible by *sp*<sup>3</sup> defects alone.

Additional experiments on complimentary systems are consistent with the three-stage relaxation model outlined above. We are currently studying films of MEH-PPV and preliminary data show that the peak shift does, in fact, decay to zero as predicted by the extremely efficient energy transfer in these films.<sup>70</sup> This energy transfer allows the system to explore all states of the ensemble.<sup>54</sup> The coupling of the electronic transitions to the solvent bath appears to be negligible compared to coupling to intramolecular modes, however, the solvent cannot be disregarded as unimportant. The solvent is known to affect the conformation of the polymer in both solution and film.<sup>114–117</sup> Furthermore, ladder-type polyparaphenylenes have been shown to obey the mirror-image rule, suggesting that the change in line shape is indeed due, at least in part, to the large geometry change in the less rigid polymers studied in this paper. The smaller Stokes' shift observed in LPPs is consistent with the model, as well. LPPs are an ideal model system to retrieve the true Stokes' shift.<sup>118,119</sup>

Some of the deviations from experimental data are readily explained. In Fig. 9, the simulated absorption spectrum does not exactly follow the experimental line shape on the red edge. In this model, we have used a Gaussian distribution of exciton states. More rigorous simulation would have us use a distribution with a steeper than Gaussian rise, which is what is observed experimentally. Also, the 3PEPS experiments are performed using laser pulses that excite on the red edge of the absorption spectrum. The blue edge is so far off-resonance that we are not sensitive to that area of the spectrum. It has been well documented that the initial part of the ultrafast decay of the 3PEPS signal is difficult to fit.<sup>91,92</sup> The underlying reason is that within the pulse-overlap region, several additional signal pathways contribute to the signal when the pulses are not properly time ordered. This is especially important in multichromophore systems and semiconductors. Coupling to high-frequency modes also affects the early time behavior of the 3PEPS signal. We are also unable to resolve accurately the frequencies of coherently excited vibrational modes that add to the 3PEPS signal.<sup>120</sup>

The implications of these results for resonance energy transfer in conjugated polymers are that there are two distinct regimes of energy migration. During the first  $\sim 25$  fs, delocalized states populated during excitation—effectively occupying several conformational subunits—are localized to a single conformational subunit. Associated spectral diffusion explains the unexpectedly rapid decay of the 3PEPS data. This relaxation is a highly complex dynamical process, wherein electronic and nuclear degrees of freedom are inseparable.<sup>86</sup> In the second, longer time scale regime prior to photoluminescence, excitation energy migrates to a subdistribution of longer conformational subunits, thus narrowing their associated spectral inhomogeneity from  $\sigma_2=425$  cm<sup>-1</sup>

to  $\sigma'_2=10$  cm<sup>-1</sup>. However, because absorption occurs to delocalized states, resonance energy transfer, in turn, operates by a non-Förster mechanism; whereby localized excitation on a donor conformational subunit transfers energy to an aggregate state. The separation of time scales between the rapid localization (25 fs) and resonance energy transfer ( $>1$  ps), suggests that such energy migration can be usefully modeled by the generalized Förster theory (GFT) models proposed recently.<sup>72,73,121–123</sup>

## VII. CONCLUSIONS

The origins of many optical properties of conjugated polymers differ greatly from those of molecular dyes and inorganic semiconductors. It is the interplay between conjugation and the conformational disorder that disrupts it that gives rise to many of these properties. We have shown that the conformational disorder in these systems results in large spectral inhomogeneity, quantified by a standard deviation,  $\sigma_2 \approx 425$  cm<sup>-1</sup>. Homogeneous line broadening results from coupling to intramolecular motions modeled by an overdamped Brownian oscillator. No evidence was found for inertial solvation. An important conclusion of our analysis was that absorption occurs from the ground state to a delocalized set of states, that we suggested originate from electronic coupling between conformational subunits. That set of states appears as an additional inhomogeneous broadening of the absorption spectrum, characterized by  $\sigma_1 \approx 416$  cm<sup>-1</sup> for MEH-PPV. The strong coupling of electronic transitions to the nuclear coordinate was suggested to be of the utmost importance in determining dynamics subsequent to photoexcitation of conjugated polymer systems. The highly nonequilibrium geometry produced upon photoexcitation—and subsequent relaxation—has a direct effect on the electronic structure of the conjugated polymer, and promotes rapid localization of excitation. This relaxation is observed in the 3PEPS experiment as a type of spectral diffusion, with  $\tau_{loc} \approx 25$  fs for MEH-PPV. The fluorescence derives from a localized state, so no trace of  $\sigma_1$  is evident in that line shape, explaining the main reason for lack of mirror image symmetry between absorption and fluorescence, as well as the large apparent Stokes' shift.

In summary, we have used the 3PEPS experiment to explore the photophysics and dynamics subsequent to photoexcitation of MEH-PPV and a model pentamer and have discussed the importance of disorder and geometry change.

## ACKNOWLEDGMENTS

The authors gratefully acknowledge Professor Lewis Rothberg for providing us with the model pentamer sample. The authors thank the Canadian Foundation for Innovation, the Ontario Innovation Trust, Research Corporation, Premiers Research Excellence Award, NSERC and Photonics Research Ontario for financial support.

\*These authors contributed equally to this work.

†Author to whom correspondence should be addressed. Electronic address: gscholes@chem.utoronto.ca

- <sup>1</sup>G. D. Scholes, D. S. Larsen, G. R. Fleming, G. Rumbles, and P. L. Burn, *Phys. Rev. B* **61**, 13670 (2000).
- <sup>2</sup>L. J. Rothberg, M. Yan, M. E. Galvin, E. W. Kwock, T. M. Miller, and F. Papadimitrakopoulos, *Synth. Met.* **80**, 41 (1996).
- <sup>3</sup>J. Cornil, D. Beljonne, R. H. Friend, and J. L. Brédas, *Chem. Phys. Lett.* **223**, 82 (1994).
- <sup>4</sup>E. Mulazzi, A. Ripamonti, J. Wery, B. Dulieu, and S. Lefrant, *Phys. Rev. B* **60**, 16519 (1999).
- <sup>5</sup>E. Mulazzi, A. Ripamonti, L. Athouël, J. Wery, and S. Lefrant, *Phys. Rev. B* **65**, 085204 (2002).
- <sup>6</sup>S. Tretiak, A. Saxena, R. L. Martin, and A. R. Bishop, *Phys. Rev. Lett.* **89**, 097402 (2002).
- <sup>7</sup>J. Bullo, B. Dulieu, and S. Lefrant, *Synth. Met.* **61**, 211 (1993).
- <sup>8</sup>G. R. Möhlmann, *Synth. Met.* **67**, 77 (1994).
- <sup>9</sup>D. R. Baigent, N. C. Greenham, J. Grüner, R. N. Marks, R. H. Friend, R. C. Moratti, and A. B. Holmes, *Synth. Met.* **67**, 3 (1994).
- <sup>10</sup>D. Oelkrug, A. Tompert, H.-J. Egelhaaf, M. Hanack, E. Steinhuber, M. Hohloch, H. Meier, and U. Stalmach, *Synth. Met.* **83**, 231 (1996).
- <sup>11</sup>H.-J. Egelhaaf, L. Lüer, A. Tompert, P. Bäuerle, K. Müllen, and D. Oelkrug, *Synth. Met.* **115**, 63 (2000).
- <sup>12</sup>E. Birckner, U. W. Grimmt, A. Hartmann, S. Pfeiffer, H. Tillmann and H.-H. Hörhold, *J. Fluoresc.* **8**, 73 (1998).
- <sup>13</sup>D. Oelkrug, A. Tompert, J. Gierschner, H.-J. Egelhaaf, M. Hanack, M. Hohloch, and E. Steinhuber, *J. Phys. Chem. B* **102**, 1902 (1998).
- <sup>14</sup>K. P. Fritz and G. D. Scholes, *J. Phys. Chem. B* **107**, 10141 (2003).
- <sup>15</sup>S. Son, A. Dodabalapur, A. J. Lovinger, and M. E. Galvin, *Science* **269**, 376 (1995).
- <sup>16</sup>K. S. Schweizer, *J. Chem. Phys.* **85**, 1156 (1986).
- <sup>17</sup>M. Schreiber and S. Abe, *Synth. Met.* **55**, 50 (1993).
- <sup>18</sup>O. Lhost and J. L. Brédas, *J. Chem. Phys.* **96**, 5279 (1992).
- <sup>19</sup>Z. G. Soos, S. Ramasesha, D. S. Galvao, and S. Etamad, *Phys. Rev. B* **47**, 1742 (1993).
- <sup>20</sup>D. S. Galvao, Z. G. Soos, S. Ramesha, and S. Etamad, *J. Chem. Phys.* **98**, 3016 (1993).
- <sup>21</sup>S. N. Yaliraki and R. J. Silbey, *J. Chem. Phys.* **104**, 1245 (1996).
- <sup>22</sup>B. E. Kohler and I. D. W. Samuel, *J. Chem. Phys.* **103**, 6248 (1995).
- <sup>23</sup>B. E. Kohler and J. C. Woehl, *J. Chem. Phys.* **103**, 6253 (1995).
- <sup>24</sup>J. Cornil, D. A. dos Santos, X. Crispins, and R. J. Silbey, *J. Am. Chem. Soc.* **120**, 1289 (1998).
- <sup>25</sup>S. Karabunarliev, M. Baumgarten, and K. Müllen, *J. Phys. Chem. A* **104**, 8236 (2000).
- <sup>26</sup>R. Chang *et al.*, *Chem. Phys. Lett.* **317**, 142 (2000).
- <sup>27</sup>G. Rossi, R. R. Chance, and R. J. Silbey, *J. Chem. Phys.* **90**, 7594 (1989).
- <sup>28</sup>J. D. White, J. H. Hsu, S.-C. Yang, W. S. Fann, G. Y. Pern, and S. A. Chen, *J. Chem. Phys.* **114**, 3848 (2001).
- <sup>29</sup>C. F. Wang, J. D. White, T. L. Lim, J. H. Hsu, S. C. Yang, W. S. Fann, K. Y. Peng, and S. A. Chen, *Phys. Rev. B* **67**, 035202 (2003).
- <sup>30</sup>M. Chandross, S. Mazumdar, M. Liess, P. A. Lane, Z. V. Vardeny, M. Hamaguchi, and K. Yoshino, *Phys. Rev. B* **55**, 1486 (1997).
- <sup>31</sup>M. H. Cho, J. Y. Yu, T. Joo, Y. Nagasawa, S. A. Passino, and G. R. Fleming, *J. Phys. Chem.* **100**, 11944 (1996).
- <sup>32</sup>W. P. de Boeij, M. S. Pshenichnikov, and D. A. Wiersma, *J. Phys. Chem.* **100**, 11806 (1996).
- <sup>33</sup>W. T. Pollard and R. A. Mathies, *Annu. Rev. Phys. Chem.* **43**, 497 (1992).
- <sup>34</sup>G. R. Fleming and M. H. Cho, *Annu. Rev. Phys. Chem.* **47**, 109 (1996).
- <sup>35</sup>T. Joo, Y. Jia, J. Y. Yu, M. Lang, and G. R. Fleming, *J. Chem. Phys.* **104**, 6089 (1996).
- <sup>36</sup>S. A. Passino, Y. Nagasawa, T. Joo, and G. R. Fleming, *J. Phys. Chem. A* **101**, 725 (1997).
- <sup>37</sup>D. S. Larsen, K. Ohta, Q. H. Xu, M. Cyrier, and G. R. Fleming, *J. Chem. Phys.* **114**, 8008 (2001).
- <sup>38</sup>K. Ohta, D. S. Larsen, M. Yang, and G. R. Fleming, *J. Chem. Phys.* **114**, 8020 (2001).
- <sup>39</sup>D. S. Larsen, K. Ohta, and G. R. Fleming, *J. Chem. Phys.* **111**, 8970 (1999).
- <sup>40</sup>M. Yan, L. J. Rothberg, E. W. Kwok, and T. M. Miller, *Phys. Rev. Lett.* **75**, 1992 (1995).
- <sup>41</sup>J. M. Leng, S. Jeglinski, X. Wei, R. E. Brenner, Z. V. Vardeny, F. Guo, and S. Mazumdar, *Phys. Rev. Lett.* **72**, 156 (1994).
- <sup>42</sup>R. Österbacka, M. Wohlgenannt, D. Chinn, and Z. V. Vardeny, *Phys. Rev. B* **60**, R11253 (1999).
- <sup>43</sup>S.-H. Lim, T. G. Bjorklund, K. M. Gaab, and C. J. Bardeen, *J. Chem. Phys.* **117**, 454 (2002).
- <sup>44</sup>T. G. Bjorklund, S.-H. Lim, and C. J. Bardeen, *J. Phys. Chem. B* **105**, 11970 (2001).
- <sup>45</sup>C. M. Heller, I. H. Campbell, B. K. Laurich, D. L. Smith, D. D. C. Bradley, P. L. Burn, J. P. Ferrais, and K. Müllen, *Phys. Rev. B* **54**, 5516 (1996).
- <sup>46</sup>S. C. J. Meskers, R. A. J. Janssen, J. E. M. Haverkort, and J. H. Wolter, *Chem. Phys.* **260**, 415 (2000).
- <sup>47</sup>T. Kobayashi, *Synth. Met.* **54**, 75 (1993).
- <sup>48</sup>C. Gadermaier *et al.*, *Phys. Rev. B* **66**, 125203 (2002).
- <sup>49</sup>J. T. M. Kennis, D. S. Larsen, K. Ohta, M. T. Facciotti, R. M. Glaeser, and G. R. Fleming, *J. Phys. Chem. B* **106**, 6067 (2002).
- <sup>50</sup>X. J. Jordanides, M. J. Lang, X. Song, and G. R. Fleming, *J. Phys. Chem. B* **103**, 7995 (1999).
- <sup>51</sup>B. J. Homoelle, M. D. Edington, W. M. Diffey, and W. F. Beck, *J. Phys. Chem. B* **102**, 3044 (1998).
- <sup>52</sup>R. Jimenez, D. A. Case, and F. E. Romesberg, *J. Phys. Chem. B* **106**, 1090 (2002).
- <sup>53</sup>M. R. Salvador, M. A. Hines, and G. D. Scholes, *J. Chem. Phys.* **118**, 9380 (2003).
- <sup>54</sup>G. R. Fleming, S. A. Passino, and Y. Nagasawa, *Philos. Trans. R. Soc. London, Ser. A* **356**, 389 (1998).
- <sup>55</sup>T. Wilhelm, J. Piel, and E. Riedle, *Opt. Lett.* **22**, 1494 (1997).
- <sup>56</sup>R. Snyder, E. Arvidson, C. Foote, L. Harrigan, and R. Christensen, *J. Am. Chem. Soc.* **107**, 4117 (1985).
- <sup>57</sup>K. L. D'Amico, C. Manos, and R. L. Christensen, *J. Am. Chem. Soc.* **102**, 1777 (1980).
- <sup>58</sup>S. Mukamel, *Principles of Nonlinear Optical Spectroscopy* (Oxford University Press, New York, 1995).
- <sup>59</sup>H. Bässler, in *Optical Techniques to Characterize Polymer Systems*, edited by H. Bässler (Elsevier, Amsterdam, 1989).
- <sup>60</sup>R. F. Mahrt and H. Bässler, *Synth. Met.* **45**, 107 (1991).
- <sup>61</sup>S. Heun, R. F. Mahrt, A. Greiner, U. Lemmer, H. Bässler, D. A. Halliday, D. D. C. Bradley, P. L. Burn, and A. B. Holmes, *J. Phys.: Condens. Matter* **5**, 247 (1993).
- <sup>62</sup>W. T. Simpson and D. L. Peterson, *J. Chem. Phys.* **26**, 588

- (1957).
- <sup>63</sup>A. Witkowski and W. Moffitt, *J. Chem. Phys.* **33**, 872 (1960).
- <sup>64</sup>M. Yang, R. Agarwal, and G. R. Fleming, *J. Photochem. Photobiol., A* **142**, 107 (2001).
- <sup>65</sup>M. H. C. Koolhaas, R. N. Frese, G. J. S. Fowler, T. S. Bibby, S. Georgakopoulou, G. van der Zwan, C. N. Hunter, and R. van Grondelle, *Biochemistry* **37**, 4693 (1998).
- <sup>66</sup>M. H. C. Koolhaas, G. van der Zwan, R. N. Frese, and R. van Grondelle, *J. Phys. Chem. B* **101**, 7262 (1997).
- <sup>67</sup>R. Monshouwer, M. Abrahamsson, F. van Mourik, and R. van Grondelle, *J. Phys. Chem. B* **101**, 7241 (1997).
- <sup>68</sup>T. Polfva, T. Pullerits, J. L. Herek, and V. Sundström, *J. Phys. Chem. B* **104**, 1088 (2000).
- <sup>69</sup>R. Jimenez, F. van Mourik, J. Y. Yu, and G. R. Fleming, *J. Phys. Chem. B* **101**, 7350 (1997).
- <sup>70</sup>M. Yang and G. R. Fleming, *J. Chem. Phys.* **111**, 27 (1999).
- <sup>71</sup>J.-Y. Yu, Y. Nagasawa, R. van Grondelle, and G. R. Fleming, *Chem. Phys. Lett.* **280**, 404 (1997).
- <sup>72</sup>G. D. Scholes and G. R. Fleming, *J. Phys. Chem. B* **104**, 1854 (2000).
- <sup>73</sup>G. D. Scholes, *Annu. Rev. Phys. Chem.* **54**, 57 (2003).
- <sup>74</sup>E. Hennebicq, G. Pourtois, G. D. Scholes, L. M. Herz, D. M. Russel, C. Silva, K. Müllen, J. L. Brédas, and D. Beljonne, presented at World Polymer Congress MACRO 2004, Paris 4 July-9 July, 2004.
- <sup>75</sup>G. R. Fleming and G. D. Scholes, *Nature (London)* **431**, 256 (2004).
- <sup>76</sup>S. H. Lin, *J. Chem. Phys.* **58**, 5760 (1973).
- <sup>77</sup>S. H. Lin and R. Bersohn, *J. Chem. Phys.* **48**, 2732 (1968).
- <sup>78</sup>P. Wood, I. D. W. Samuel, R. Schrock, and R. L. Christensen, *J. Chem. Phys.* **115**, 10955 (2001).
- <sup>79</sup>Y. R. Shen, *The Principles of Nonlinear Optics* (Wiley, New York, 1984).
- <sup>80</sup>W. B. Bosma, Y. J. Yan, and S. Mukamel, *Phys. Rev. A* **42**, 6920 (1990).
- <sup>81</sup>S. Mukamel, *Phys. Rev. A* **28**, 3480 (1983).
- <sup>82</sup>Y. J. Yan and S. Mukamel, *J. Chem. Phys.* **89**, 5160 (1998).
- <sup>83</sup>C. H. Chang *et al.*, *Synth. Met.* **106**, 139 (1999).
- <sup>84</sup>R. M. Stratton and M. Cho, *J. Chem. Phys.* **100**, 6700 (1994).
- <sup>85</sup>M. Maroncelli and G. R. Fleming, *J. Chem. Phys.* **89**, 875 (1988).
- <sup>86</sup>R. Chang, M. Hayashi, S. H. Lin, J. H. Hsu, and W. S. Fann, *J. Chem. Phys.* **115**, 4339 (2001).
- <sup>87</sup>M. M.-L. Grage, T. Pullerits, A. Rusekas, M. Theander, O. Inganäs, and V. Sundström, *Chem. Phys. Lett.* **339**, 96 (2001).
- <sup>88</sup>D. Beljonne, G. Pourtois, C. Silva, E. Hennebicq, L. M. Herz, R. H. Friend, G. D. Scholes, S. Setayesh, K. Müllen, and J. L. Brédas, *Proc. Natl. Acad. Sci. U.S.A.* **99**, 10982 (2002).
- <sup>89</sup>R. Kubo, *Adv. Chem. Phys.* **15**, 101 (1969).
- <sup>90</sup>J. Sue, Y. J. Yan, and S. Mukamel, *J. Chem. Phys.* **85**, 462 (1986).
- <sup>91</sup>W. M. Zhang, T. Meier, V. Chernyak, and S. Mukamel, *J. Chem. Phys.* **108**, 7763 (1998).
- <sup>92</sup>W. M. Zhang, T. Meier, V. Chernyak, and S. Mukamel, *Philos. Trans. R. Soc. London, Ser. A* **356**, 405 (1986).
- <sup>93</sup>D. Wexler, G. G. Kochendoerfer, and R. A. Mathies, in *Femtochemistry and Femtobiology: Ultrafast Reaction Dynamics at Atomic Scale Resolution*, edited by V. Sundström (Imperial College Press, London, 1997).
- <sup>94</sup>R. Kersting, U. Lemmer, R. F. Mahrt, K. Leo, H. Kurz, H. Bässler, and E. O. Göbel, *Phys. Rev. Lett.* **70**, 3820 (1993).
- <sup>95</sup>H. Bässler and B. Schweitzer, *Acc. Chem. Res.* **32**, 173 (1999).
- <sup>96</sup>B. Carmeli and D. Chandler, *J. Chem. Phys.* **82**, 3400 (1985).
- <sup>97</sup>J. N. Gehlen, D. Chandler, H. J. Kim, and J. T. Hynes, *J. Phys. Chem.* **96**, 1748 (1992).
- <sup>98</sup>T.-Q. Nguyen, J. Wu, V. Doan, B. J. Schwartz, and S. H. Tolbert, *Science* **288**, 652 (2000).
- <sup>99</sup>B. J. Schwartz, *Annu. Rev. Phys. Chem.* **54**, 141 (2003).
- <sup>100</sup>D. Beljonne, G. Pourtois, Z. Shuai, E. Hennebicq, G. D. Scholes, and J. L. Brédas, *Synth. Met.* **137**, 1369 (2003).
- <sup>101</sup>H. Weisenhofer, D. Beljonne, G. D. Scholes, E. Hennebicq, J. L. Brédas, and E. Zojer, *Adv. Funct. Mater.* (in press).
- <sup>102</sup>E. Zojer, A. Pogantsch, E. Hennebicq, D. Beljonne, J. L. Brédas, P. S. de Freitas, U. Scherf, and E. J. W. List, *J. Chem. Phys.* **117**, 6794 (2002).
- <sup>103</sup>A. B. Myers, *J. Opt. Soc. Am. B* **7**, 1665 (1995).
- <sup>104</sup>A. B. Myers, *J. Raman Spectrosc.* **28**, 389 (1997).
- <sup>105</sup>S. Mukamel, S. Tretiak, T. Wagersreiter, and V. Chernyak, *Science* **277**, 781 (1997).
- <sup>106</sup>J. L. Brédas, J. Cornil, D. Beljonne, D. A. dos Santos, and Z. Shuai, *Acc. Chem. Res.* **32**, 267 (1999).
- <sup>107</sup>S. Tretiak and S. Mukamel, *Chem. Rev. (Washington, D.C.)* **102**, 3171 (2002).
- <sup>108</sup>A. Köhler, D. A. dos Santos, D. Beljonne, Z. Shuai, J. L. Brédas, A. B. Holmes, A. Kraus, K. Müllen, and R. H. Friend, *Nature (London)* **392**, 903 (1998).
- <sup>109</sup>W. J. D. Beenken and T. Pullerits, *J. Phys. Chem. B* **108**, 6164 (2004).
- <sup>110</sup>S. Karabunarliev and E. B. Bittner, *J. Chem. Phys.* **118**, 4291 (2003).
- <sup>111</sup>A. Z. Szarka, N. Pugliano, D. K. Palit, and R. M. Hochstrasser, *Chem. Phys. Lett.* **240**, 25 (1995).
- <sup>112</sup>R. J. Senison, S. T. Repinec, A. Z. Szarka, and R. M. Hochstrasser, *J. Chem. Phys.* **98**, 6291 (1993).
- <sup>113</sup>P. Geissinger, B. E. Köhler, S. G. Kulikov, and V. Terpougov, *J. Chem. Phys.* **108**, 1821 (1998).
- <sup>114</sup>J. Yu, D. Hu, and P. F. Barbara, *Science* **289**, 1327 (2000).
- <sup>115</sup>D. Hu, J. Yu, K. Wong, B. Bagchi, P. J. Rossky, and P. F. Barbara, *Nature (London)* **405**, 1030 (2000).
- <sup>116</sup>T.-Q. Nguyen, V. Doan, and B. J. Schwartz, *J. Chem. Phys.* **110**, 4068 (1999).
- <sup>117</sup>S. E. Shaheen, C. J. Brabec, N. S. Sariciftci, F. Padinger, T. Fromherz, and J. C. Hummelen, *Appl. Phys. Lett.* **78**, 841 (2001).
- <sup>118</sup>J. G. Müller, U. Lemmer, G. Raschke, M. Anni, U. Scherf, J. M. Lupton, and J. Feldmann, *Phys. Rev. Lett.* **91**, 267403 (2003).
- <sup>119</sup>T. Pauck, H. Bässler, J. Grimme, U. Scherf, and K. Müllen, *Chem. Phys.* **210**, 219 (1996).
- <sup>120</sup>G. Lanzani, G. Cerullo, C. Brabec, and N. S. Sariciftci, *Phys. Rev. Lett.* **90**, 047402 (2003).
- <sup>121</sup>G. D. Scholes, X. J. Jordanides, and G. R. Fleming, *J. Phys. Chem. B* **105**, 1640 (2001).
- <sup>122</sup>H. Sumi, *J. Phys. Chem. B* **103**, 252 (1999).
- <sup>123</sup>S. Jang, M. D. Newton, and R. J. Silbey, *Phys. Rev. Lett.* **92**, 218301 (2004).